On applicability of spheroidal shapes to describe observed cloud radar depolarization ratios of ice hydrometeors

Scanning W-band radar

Sergey Y. Matrosov

Cooperative Institute for Research in Environmental Sciences, University of Colorado and NOAA Earth Sciences Research Laboratory, 325 Broadway, Boulder, Colorado 80305, USA

(Dated: 1 July 2014)

1 Introduction

Depolarization ratio (DR) is a common variable measured by cloud radars. It has been shown experimentally with nearly collocated cloud radar and in situ ice particle observations that different types of K_a- and W-band DR values and their elevation angle trends can be used to distinguish among columnar and planar types of crystals and their aggregates (e.g., Matrosov et al. 2001, 2012; Reinking et al.2002). Microphysical in situ data (e.g., Korolev and Isaac 2002) show that pristine crystal shapes (e.g., dendrites, needles, etc.) describe a relatively small fraction of observed particles, a majority of which have irregular nonspherical shapes. An aspect ratio parameter, *r*, is often used to describe particle nonsphericity.

The simplest shape model that accounts for general nonsphericity is the spheroidal model. The aspect ratio in this model (i.e. the ratio of particle smallest and largest dimensions) describes a particle degree of nonsphericity, while oblate/prolate spheroids are used to represent planar/columnar ice hydrometeors. Using experimental data, this model has been previously shown to adequately describe radar dual-wavelength ratio (DWR) and differential reflectivity in ice clouds (e.g., Matrosov et al. 2005a, Hogan et al. 2012). Recent studies with more sophisticated aggregate ice particle models and computational approaches (e.g., Leinonen et al. 2012) indicated that in some cases for larger particle populations resulting in high values of DWR, the spheroidal model may not provide consistency for DWR values over multiple radar wavelengths. However, as shown by these authors for other experimental cases the spheroidal model can explain DWR radar observations while more sophisticated models cannot.

Recent studies with complex models (e.g. Petty and Huang 2010; Botta et al. 2011; Tyynela et al. 2011; Hogan and Westbrook 2014) indicated also that for individual large ice particles, the use of the spheroidal model can result in significant underestimation of backscatter cross sections. The backscatter errors are more pronounced for higher frequencies and are attributable to existence of resonance minimums in the spheroidal model backscatter. For particle populations resonance influences are much reduced due to size integration. As a result, the spheroidal model backscatter is often in reasonable agreement with a range predicted by more sophisticated particle shapes (Liu 2008) and provides for larger particle populations such as snowfall (Matrosov 2007) W-band reflectivity values up to about 15 dBZ, which is close to largest observed values at this frequency band (e.g., Liu 2008). It has been also shown (Hogan and Westbrook 2014, their Fig. 5) that particle populations of more complex shape aggregates and spheroids of the same mass and aspect ratios provide similar W-band backscatter. While the differences between these two particle model backscatter generally increase with reflectivity, even for highest reflectivities (i.e., larger characteristic sizes) these differences are similar to the backscatter variability caused by a reasonable uncertainty in aspect ratios for the same particle model (e.g., 0.5 vs 0.6). An objective of this study was to assess a utility of the spheroidal model for describing depolarization caused by ice hydrometeors. This study uses observations at W-band, which is the highest (i.e., the most challenging for modeling) frequency utilized by meteorological radars, using data collected by a scanning W-band Atmospheric Radiation Measurement (ARM) cloud radar (SWACR) in diverse ice cloud and precipitation conditions during the Storm Peak Validation Experiment – StormVEx (Mace et al. 2010).

2. Theoretical background

Many cloud radars operating at mm-wavelengths, including those from the ARM Program, transmit a single polarization signal and receive co-polar and cross-polar components of the backscattered echo. The vector of voltages of these components (V_{co} and V_{cr}, correspondingly) in the presence of unavoidable radar system cross-coupling can be expressed as (e.g., Zrnic et al. 2010):

$$\begin{bmatrix} V_{co} \\ V_{cr} \end{bmatrix} = \mathbf{F}^{\mathrm{T}}\mathbf{B}\mathbf{F}\,\mathbf{E}_{\mathrm{i}} = \begin{bmatrix} F_{11} & F_{21} \\ F_{12} & F_{22} \end{bmatrix} \begin{bmatrix} B_{11} & B_{12} \\ B_{21} & B_{22} \end{bmatrix} \begin{bmatrix} F_{11} & F_{12} \\ F_{21} & F_{22} \end{bmatrix} \begin{bmatrix} 1 \\ 0 \end{bmatrix} \quad (1)$$

where the superscript $^{\mathrm{T}}$ denotes the transpose matrix, **B** and **F** represent the target backscatter amplitude and the radar system cross-coupling matrices, respectively, and the last term in (1) represents the transmitted unit electrical vector. For the traditional horizontal - vertical (*h*-*v*) polarization basis in the case of hydrometeor backscatter, the elements of the matrix **B** for a spheroid can be expressed as (e.g., Bringi and Chandrasekar 2001):

$$B_{11} = B_{hh} = S_{hh}\cos^2\alpha + S_{vv}\sin^2\alpha \quad (2a)$$
$$B_{12} = B_{21} = B_{hv} = 0.5(S_{vv} - S_{hh})\sin 2\alpha \quad (2b)$$
$$B_{22} = B_{vv} = S_{vv}\cos^2\alpha + S_{hh}\sin^2\alpha, \quad (2c)$$

where α is the apparent canting angle (i.e., the projection of the hydrometeor axis zenith angle on the incident wave polarization plane), and S_{hh} and S_{vv} are the zero canting complex backscatter amplitudes along the unit vectors of the horizontal and vertical polarization, respectively. The normalizing terms are omitted because they do not influence radar variables which are considered (i.e., reflectivity logarithmic differences and depolarization). These equations are written in the backscatter alignment (BSA) convention, where S_{hh} and S_{vv} generally have the same sign. Note that in the optical convention, which is also widely used, they have the opposite signs (e.g., $S_{hh} = -S_{vv}$ for a sphere) and $B_{21} = -B_{12}$. The media transmission (e.g., differential phase on propagation) effects are neglected here because further comparisons are performed for short observational ranges (i.e., few kilometers). Attenuation in dry ice is generally negligible, and attenuation in atmospheric gases and in cloud liquid composed of small spherical drops is the same for both orthogonal polarizations thus not affecting DR.

The backscatter matrix in the slant linear polarization basis $\mathbf{B_{sl}}$ can be obtained from the *h*-*v* backscatter matrix $\mathbf{B_{hv}}$ as

$$\mathbf{B_{sl}} = \mathbf{R}(-\gamma)\,\mathbf{B_{hv}}\,\mathbf{R}(\gamma) \tag{3}$$

where the rotation matrix $\mathbf{R}(\gamma)$ is given by

$$\mathbf{R}(\gamma) = \begin{bmatrix} \cos\gamma & \sin\gamma \\ -\sin\gamma & \cos\gamma \end{bmatrix} \tag{4}$$

For the slant 45° (γ=45°) polarization basis, which is sometimes used with cloud radars, rotating according to (3) and (4) provides for the matrix elements in (1):

$$B_{11} = 0.5S_{hh} + 0.5S_{vv} + (S_{hh} - S_{vv})\sin\alpha\cos\alpha \tag{5a}$$
$$B_{12} = B_{21} = 0.5\,(S_{hh} - S_{vv})\cos 2\alpha \tag{5b}$$
$$B_{22} = 0.5S_{hh} + 0.5S_{vv} - (S_{hh} - S_{vv})\sin\alpha\cos\alpha \tag{5c}$$

The backscatter matrix in the circular polarization basis $\mathbf{B_c}$ can be obtained from the *h*-*v* backscatter matrix $\mathbf{B_{hv}}$ as

$$\mathbf{B_c} = \mathbf{C}^{-1}\,\mathbf{B_{hv}}\,\mathbf{C} \tag{6}$$

where the matrix $\mathbf{C}$ is given by

$$\mathbf{C} = 0.5^{1/2} \begin{bmatrix} 1 & 1 \\ j & -j \end{bmatrix} \tag{7}$$

The corresponding matrix elements for circular polarization are

$$B_{11} = 0.5(S_{hh} - S_{vv})\exp(-2j\alpha) \tag{8a}$$
$$B_{12} = B_{21} = 0.5(S_{hh} + S_{vv}) \tag{8b}$$
$$B_{22} = 0.5(S_{hh} - S_{vv})\exp(2j\alpha) \tag{8c}$$

where $j^2 = -1$. As seen from (8) the main power return in the circular polarization basis comes in the cross-polarization receiver channel.

The trigonometric functions of the apparent canting angle α are related to the particle axis orientation zenith, θ (i.e., the true canting angle with respect to the local vertical) and azimuthal, ϕ, angles, and radar elevation angle χ in the following way

$$\cos\alpha\,\sin\psi = \cos\theta\,\cos\chi + \sin\theta\,\sin\chi\,\cos\phi \tag{9a}$$
$$\sin\alpha\,\sin\psi = \sin\theta\,\sin\phi \tag{9b}$$
$$\cos\psi = \cos\theta\,\sin\chi - \sin\theta\,\cos\beta\,\cos\phi \tag{9c}$$

where ψ is the particle axis orientation angle with respect to the propagation direction of the incidence electromagnetic wave. The matrix elements S_{hh} and S_{vv} for non-canted in the polarization plane spheroidal particles can be calculated using the T-matrix method for different radar elevation angles.

In the radar system cross-coupling matrix $F_{11}=F_{22}$ and after the normalization of this matrix by the value of the diagonal elements, the transmit/receive isolation can be expressed by a small, complex cross-talk term ε (Bringi and Chandrasekar 2001) representing off-diagonal elements of this matrix. The depolarization ratio (DR) in the linear bases is then can expressed as

$$DR = 10\log_{10}(\langle|V_{cr}|^2\rangle/\langle|V_{co}|^2\rangle) = 10\log_{10}[\langle|B_{12}+\varepsilon(B_{11}+B_{22})+\varepsilon^2 B_{12}|^2\rangle/\langle|B_{11}+2\varepsilon\,B_{12}+\varepsilon^2 B_{22}|^2\rangle], \tag{10}$$

where angular brackets denote integration over hydrometer size and canting angle distributions. Small terms containing $\varepsilon^2 B_{12}$ in the nominator and $\varepsilon^2 B_{22}$ in the denominator can be safely neglected. The second term in the denominator also can be neglected because for most practical cases the co-polar echo signals are much stronger than cross-polar signals and $|B_{11}| >> 2|\varepsilon B_{12}|$. These simplifications yield:

$$DR \approx 10\log_{10}\{(\langle|B_{12}|^2\rangle + |\varepsilon|^2\langle|B_{11}+B_{22}|^2\rangle + 2\mathrm{Re}[\langle(B_{11}+B_{22})B_{12}^{*}\rangle\varepsilon])/\langle|B_{11}|^2\rangle\}, \tag{11}$$

where * is the complex conjugate sign. The third term in the nominator of (11) averages to zero due to reflection symmetry (e.g.,Bringi and Chandrasekar 2001) providing further simplification:

$$DR \approx 10\log_{10}[(\langle|B_{12}|^2\rangle + |\varepsilon|^2\langle|B_{11}+B_{22}|^2\rangle)/\langle|B_{11}|^2\rangle]. \tag{12}$$

Eq. (12) is written for the linear polarization basis. Substitutions in (12) $B_{11}+B_{22} \rightarrow 2B_{12}$ and $B_{11} \leftrightarrow B_{12}$ provide estimates of DR in the circular polarization basis. The term $|\varepsilon|^2$ can be estimated from measurements in drizzle (i.e., almost perfect spheres) for which $B_{11}=B_{22}$ and $B_{12}=0$. For the SWACR, which was operated during StormVEx field project in the slant-45° linear polarization mode, it was estimated that $|\varepsilon| \approx 0.0406$, which corresponds to the minimal DR_{min} of about -21.8 dB.

3. Comparisons of modeled and observed cloud radar depolarization measurements

Particle populations were modeled using the exponential distribution, $N(D) = N_o \exp(-3.67D/D_o)$, which usually describes larger particles contributing to the total reflectivity most rather well. For relative variables such as DR and reflectivity differences in the decibel scale, the intercept of the exponential distribution is not important, so a single distribution parameter – the median volume particle size, D_o, was considered here. Due to aerodynamic forcing particles are on average oriented with their major dimensions in the horizontal plane (i.e., the mean canting angle $\theta_{mean}=0^o$). Typical standard deviations of θ (σ_θ), which describes particle flutter, for dendrite-type oblate particles are about 8°-9°, as independent measurements based on different polarimetric radar variables indicate (Matrosov et al. 2005b; Melnikov and Straka 2013). It is assumed hereafter that the distribution of particle axes is Gaussian with respect to the zenith angle θ and random with respect to the azimuthal angle ϕ. The maximal size used in integration over particle populations was 1 cm.

For the DR_{min}= -21.8 dB, Fig. 1a shows some calculated elevation angle dependences of different depolarization ratios including traditional linear depolarization ratio when horizontal polarization is transmitted (HLDR), slant-45° linear depolarization ratio (SLDR), and circular depolarization ratio (CDR). It can be seen that for modest values of σ_θ, CDR and SLDR are similar (although CDR is generally higher) and do not significantly depend on particle flutter σ_θ given that this flutter remains relatively modest. Note that CDR and SLDR are identical for non-canted hydrometeors as it could be seen from comparing equations (5) and (8). In contrast to SLDR and CDR, HLDR values are very low and there is significant variability depending on σ_θ. For DR_{min}= −21.8 dB and $\sigma_\theta < 15^o$, expected HLDR values are barely detectable even at slant viewing. Modeling using the spheroidal shapes approximate observed DR trends quite well, although as indicated by Matrosov et al. (2012) different sets of characteristic particle sizes/densities and aspect ratios can provide similar SLDR elevation angle patterns. More experimental examples of SWCR measurements are shown by Matrosov et al. (2012) and Marchand et al. (2013). Fig. 1b shows the depolarization ratio elevation angle for a better cross-polarization isolation with DR_{min}= −28 dB. This isolation level was characteristic for the SWACR when it was operated in the traditional *h-v* polarization basis. The SWACR conversion from the *h-v* polarization scheme to the slant-45° scheme inadvertently resulted in a loss in the system cross-polar isolation (i.e., −21.8 dB vs −28 dB). It can be seen from Fig. 2b that for DR_{min}= −28 dB HLDR values could be better detectable (given that the cross-polarized signals are above the noise level), though there is still quite a strong dependence of HLDR on hydrometeor flutter σ_θ.

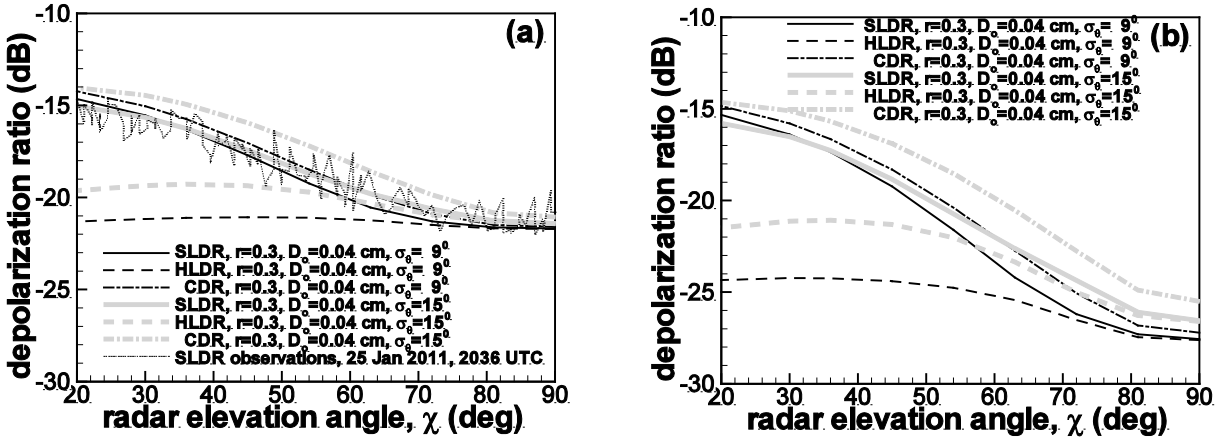

Figure 1: Comparisons of model results of different depolarization ratio elevation angle dependencies with observations for the SWACR cross-talk of -21.8 dB (a) and modeling results assuming the -28 dB cross-talk (b). The m-D relation from Brown and Francis (1995) and the particle aspect ratio r=0.3 were assumed.

As depolarization ratios, co-polar reflectivity of oriented nonspherical hydrometeors, Z_{co}, depends on the direction of viewing. Changes in observed Z_{co} as a function of radar elevation angle are particularly large at W-band, which is explained, in part, by non-Rayleigh scattering (Matrosov et al. 2005a). Differences between zenith and slant viewing values of Z_{co} during StormVEx were as large as about 12 dB during some events when single dendritic and/or plate crystals were a dominant particle habit (e.g., Matrosov et al. 2012; Marchand et al. 2013). While the oblate spheroidal model was able to generally predict patterns of the off-zenith reflectivity decrease (Matrosov et al. 2012), the meaningful comparisons were hampered by the fact that attenuation due to supercooled liquid water and atmospheric gases, while not a factor for depolarization measurements, generally enhances the magnitude of reflectivity decreasing trends.

Marchand et al. (2013) analyzed the StormVEx SWACR data set selecting cases with relatively homogenous cloud conditions. For such cases, they corrected for attenuation effects using a symmetry of the range-height indicator (RHI) scan measurements and determined observational estimates of non-attenuated values of the reflectivity zenith enhancement ΔZ_{co},

which is defined as the logarithmic difference between reflectivities in the zenith (χ=90°) and slant ($\chi \approx 25°$-35°) directions. The estimated from observations values of ΔZ_{co} were found to strongly correlate (the correlation coefficient being 0.79) with the observed SLDR differences between zenith and slant viewing. A specific difference

$$\Delta\text{SLDR} = \text{SLDR}(90°) - \text{SLDR}(45°) \quad (13)$$

was considered in the Marchand et al. (2013) study to relate observational values of ΔSLDR and ΔZ_{co} (their Fig.5).

StormVEx observations of ΔZ_{co} and ΔSLDR, which are largely free of attenuation effects, present a convenient data set for testing a spheroidal particle model. Theoretical values of ΔZ_{co} and ΔSLDR were calculated using this model and different mass – size relations, which determine particle bulk density. The attenuation-free reflectivity enhancements were estimated using (5a) from the expression

$$\Delta Z_{co} = 10 \log_{10} [\langle |B_{11}(90°)|^2 \rangle / \langle |B_{11}(30°)|^2 \rangle]. \quad (14)$$

The model particle aspect ratios varied from 1 (i.e., spheres) to 0.2. Smaller aspect ratios, while likely being more appropriate for pristine habits such as dendrites and plates, were not modeled since the T-matrix method for calculating complex scattering amplitudes of such particles becomes increasingly unstable especially for larger sizes.

For the oblate spheroid particle model, Fig.2 shows the results of simulations of the correspondence between ΔZ_{co} and ΔSLDR. The ΔSLDR computations were performed using (12) and (5) assuming the mass-size relations shown in Fig.1 and three different values of the median volume particle size (0.04, 0.08 and 0.12 cm). Such characteristic distribution sizes were typical during StormVEx observations according to the measurements from Droplet Measurement Technologies (DMT) cloud and precipitation measurement probes which were part of the StormVEx instrument suite. While the particle orientation flutter for data in Fig.2 was assumed to be σ_θ=9°, there is little variation of results when σ_θ varies between 0°, which corresponds to particle alignment with the major dimension in the horizontal plane, and 20°. The data that correspond to different values of aspect ratio *r* change along the curves depicted in Fig. 2 with spheres corresponding to the graph origin, where ΔZ_{co} = ΔSLDR = 0 dB. Data points for aspect ratios of 0.2 correspond to the end of the curves in this figure.

The area of general observational data scatter between ΔZ_{co} and ΔSLDR from Marchand et al. (2013) is also shown in Fig. 2. While this scatter area is rather large, about 90% of all data points were characterized by ΔZ_{co}<6 dB and belong to the sub-area in Fig. 2 where the theoretical curves are located. The data area with larger ΔZ_{co} values, which is not generally covered by theoretical curves, corresponds to particles with very high degree of nonsphericity. Such particles were not modeled here due to the T-matrix method application restrictions mentioned above. As seen from Fig. 2, for the given mass-size relations and ΔSLDR, particle populations with larger D_o are expected to produce more significant zenith reflectivity enhancements.

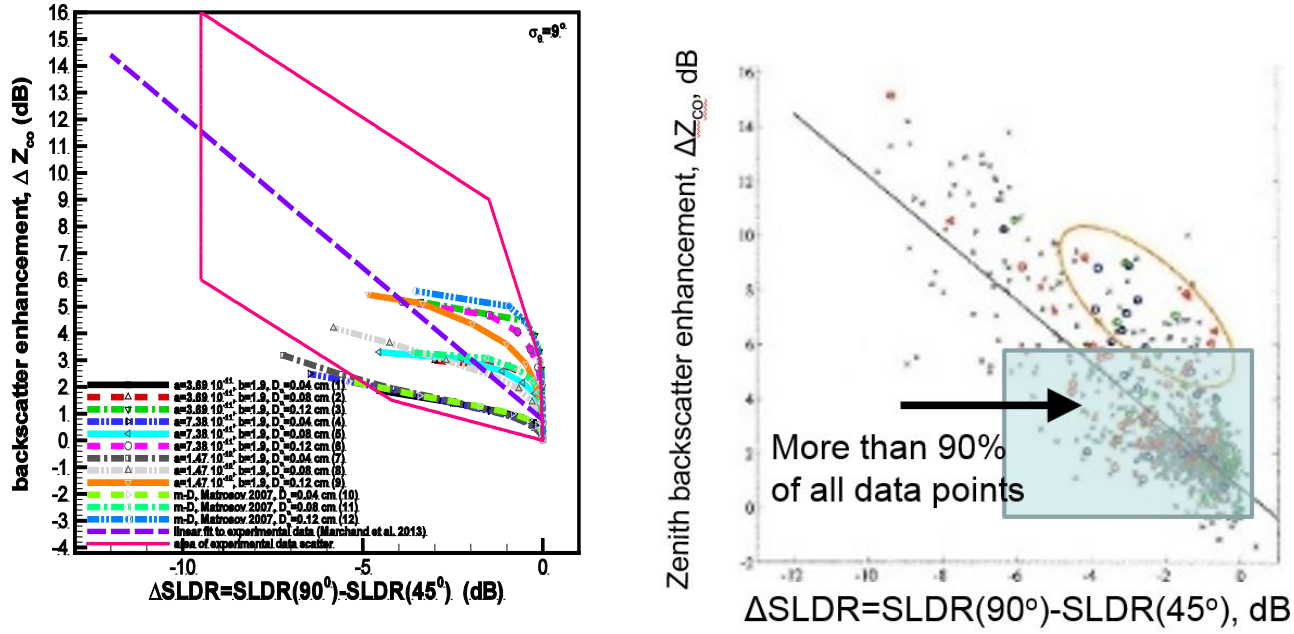

Figure 2: Left: simulations of backscatter enhancement versus SLDR difference for spheroidal particles for different mass-size relations and aspect ratio assumptions. Aspect ratio change along the curves shown from 1 at the (0.,0.) point to 0.2 at the end of each curve. Different curves correspond to different assumptions in the coefficients in the particle mass-size relations $m=aD^b$ (D is in microns and m is in grams, curves 4-6 correspond to the Brown and Francis 1995 relation) and different D_o.

Right: Experimental data scatter plot of backscatter enhancements vs SLDR differences from StormVEx (adopted from Marchand et al. 2013).

As the comparisons described above show, the theoretical estimates of the correspondence between ΔZ_{co} and ΔSLDR agree relatively well with observational quantities when reasonable assumptions about particle aspect ratios and mass-size relations are made. These results indicate that a spheroidal particle model may satisfactorily describe the depolarization properties and corresponding zenith direction backscatter enhancements observed in ice clouds and precipitation. Since the spheroidal model also describes particle nonsphericity using a single aspect ratio parameter, it is convenient to describe particles using this model. While such a description is obviously a certain simplification, particle shapes are often diverse and irregular, thus it is not generally clear without further detailed studies if the use of a particular more sophisticated not-pristine particle model can adequately describe the multiplicity of real shapes.

4. Potential for inferring particle aspect ratio from radar depolarization measurements

It can be concluded from Fig. 2 that the observed SLDR differences and backscatter enhancements can be described using different mass-size relations and aspect ratios. The aspect ratio estimates are needed for better representation of ice hydrometeor in cloud and climate models and also for enhancements of remote sensing methods that typically simply assume particle shapes. It is instructive to briefly evaluate potentials for particle aspect ratio retrievals using depolarization measurements in a framework of the simplified spheroidal model. The measurements using slant-45° linear or circular polarizations are suitable for this purpose, since they depend on particle flutter parameter (i.e., σ_θ) relatively insignificantly. Since implementation of the slant-45° linear polarization is generally easier to perform in practice, the use of SLDR measurements is analyzed here.

Figure 3a shows particle aspect ratio, *r* as a function of ΔSLDR for different mass-size relations from Fig.2 and different values of D_o. The median reflectivity enhancement measured during StormVEx was 2.4 dB, which corresponds to the median observational value ΔSLDR of −1.4 dB (Marchand et al. 2013). For the mass-size relation with coefficients used by Brown and Francis (1995) and for a median volume particle size of 0.04 cm, the corresponding value of *r* is approximately 0.52, which is not significantly different from the mean value from a large experimental aircraft-based data set (Korolev and Isaac 2003). The range of SLDR changes is greater if depolarization at more slant viewing than 45° is compared to the zenith values, so the "depolarization difference signal", which is used for aspect ratio estimations, is stronger. To illustrate this fact Fig. 3b shows relations between *r* and Δ_1SLDR defined as a positive difference between SLDR at radar elevation angles χ=30° and 90°:

$$\Delta_1\text{SLDR} = \text{SLDR}(30^o) - \text{SLDR}(90^o). \quad (15)$$

Analyzing the data in Fig. 3b can provide some measure of errors which can be expected when estimating particle aspect ratios under the oblate spheroidal model when there are factor of 2 uncertainties in both *m-D* relations and the distribution characteristic size. It can be seen, for example, that Δ_1SLDR of about 2 dB, which corresponds to the median observed value ΔSLDR of −1.4 dB in StormVEx, can be produced by particles with aspect ratios *r* ranging from about 0.3 to 0.65. If Δ_1SLDR is greater than about 4 dB/ 8dB, particles are expected to have *r* values less than about 0.5/0.3. The larger aspect ratios (i.e., more spherical particles) for a given Δ_1SLDR value correspond to denser particles. For Δ_1SLDR<6 dB, a mean relation approximating a family of curves in Fig. 3b (for the StormVEx SWACR configuration) can be given as

$$r \approx 0.5\,(\Delta_1\text{SLDR})^{-0.2}\,. \quad (17)$$

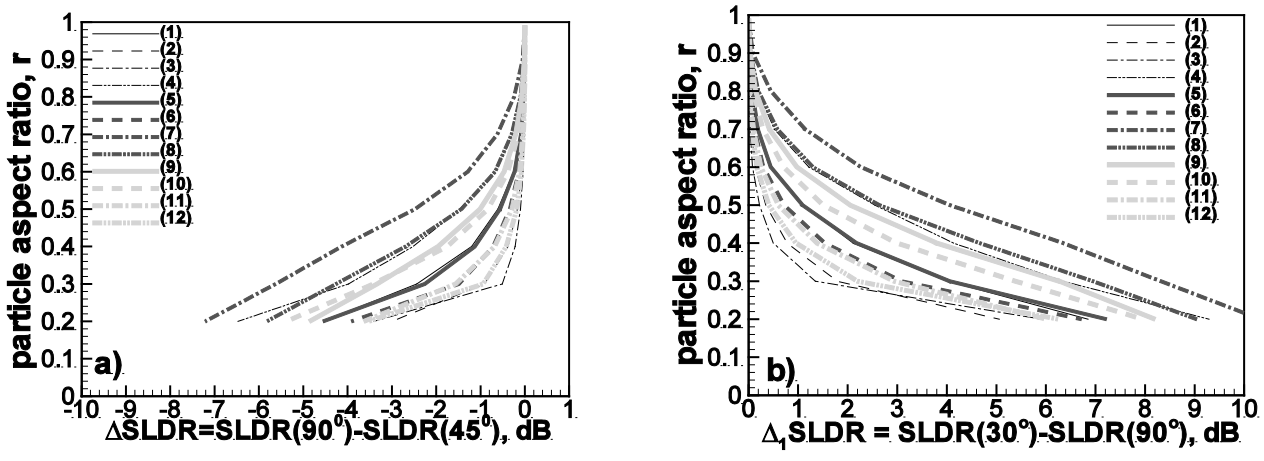

Figure 3: Relations between particle aspect ratio and SLDR slant vs zenith viewing differences (90° vs 45° - a, 30° vs 90° - b) for different mass-size relations and characteristic particle sizes. Numbers for combinations of m-D relations and D_o are the same as in Fig. 2

4. Conclusions

The simplest nonspherical shape used for hydrometeor modeling is that of a spheroid. It has only one parameter (i.e., aspect ratio) describing particle shapes besides a general spheroid type (i.e., oblate vs prolate). Modeling W-band depolarization ratios and zenith reflectivity enhancements of ice hydrometeor distributions characterized by varying particle mass-size relations and median volume sizes provides results that are in general agreement with observations from the scanning cloud radar in differing ice cloud and precipitation conditions.

The use of depolarization ratio (DR) measurements was evaluated for potential estimates of the particle aspect ratio under the assumed spheroidal model. While CDR measurements are least sensitive to particle orientations and generally have higher values (i.e., stronger signals in the "weak" polarization receiver channel), SLDR values are expected to be similar to those of CDR when hydrometeor "flutter" around their aerodynamically forced preferential orientation with major dimensions in the horizontal plane is relatively small. Depolarization measurements using traditional horizontal and vertical polarizations (i.e., HLDR) show significant dependence on particle flutter (i.e., on σ_θ). Under the oblate spheroidal model assumption, particle aspect ratios may potentially be estimated from the differences of SLDR values at slant (e.g., a 30^o elevation) and zenith viewing. While these estimations do not require an assumption of homogeneous cloud layers, there is an assumption that particle habits are generally the same at slant and zenith viewing. Errors of these estimations are expected to be significant. For a factor of two uncertainties in the distribution characteristic size (e.g., median volume size) and particle mass-size relations, aspect ratios of about 0.5 ± 0.2 could be expected for the median SLDR difference observed by the SWACR during StormVEx. Estimated aspect ratios would represent an effective value for the whole particle distribution.

The relatively large StormVEx data set (Matrosov et al. 2012; Marchand et al. 2013) indicated that the dominant planar hydrometeor habits were observed during a majority of experimental events, which were characterized by the increasing SLDR trend as radar viewing was changing from zenith to slant directions. The presence of columnar crystal types in mixtures, which are still dominated by planar crystals, does not significantly alter this trend (even though there could be an offset from minimal depolarization values, so SLDR changes with radar elevation angle are indicative of the dominant planar crystal aspect ratios. Rare StormVEx experimental events with a dominance of columnar crystal types were characterized by significant SLDR offsets and nearly neutral elevation angle SLDR dependencies. For these situations, a prolate spheroidal model might be appropriate for future developments of remote sensing methods of particle shape estimations.

References

Bringi, V. N., and V. Chandrasekar, 2001: *Polarimetric Doppler Weather Radar*. Cambridge University Press, 636 pp.

Brown, P.R.A., and P.N. Francis, 1995: Improved measurements of the ice water content in cirrus using total-water probe. *J. Atmos. Oceanic Technol*., **12**, 410–414.

Botta, G., K. Aydin, J. Verlinde, A. E. Avramov, A. S. Ackerman, A. M. Fridlind, G. M. McFarquhar, and M. Wolde , 2011: Millimeter wave scattering from ice crystals and their aggregates: Comparing cloud model simulations with X- and Ka-band radar measurements. *J. Geophys. Res*., **116**, D00T04, doi:10.1029/2011JD015909.

Hogan, R. J., L. Tian, P. R. A. Brown, C. D. Westbrook, A. J. Heymsfield, and J. D. Eastment, 2012: Radar scattering from ice aggregates using the horizontally aligned oblate spheroid approximation. *J. Appl. Meteor. Climatol*., **51**, 655–671.

Hogan, R.J., and C.D. Westbrook, 2014: Equation for the microwave backscatter cross section of aggregate snowflakes using the self-similar Rayleigh-Gans approximation. *J. Atmos. Sci*., in press.

Korolev, A.V., and G. Isaac, 2003: Roundness and aspect ratio of particles in ice clouds. *J. Atmos. Sci*., **60**, 1795-1808.

Leinonen, J., S. Kneifel, D. Moisseev, J. Tyynelä, S. Tanelli, and T. Nousiainen, 2012: Evidence of nonspheroidal behavior in millimeter-wavelength radar observations of snowfall. *J. Geophys. Res*., **117**, D18205, doi:10.1029/2012JD017680.

Liu, G., 2008: Deriving snow cloud characteristics from CloudSat observations. *J. Geophys. Res*., **113**, D00A09, doi:10.1029/2007JD009766.

Mace, G., S. Matrosov, B. Orr, M. Shupe, R. Coulter, A. Sedlacek, A.G Hallar, L. Avallone, I. McCubbin, C. Long, R. Marchand, and P. Lawson, 2010: STORMVEX: The Storm Peak Lab Cloud Property Validation Experiment Science and Operations Plan, US Dept. of Energy, DOE/SC-ARM-10-021.

Marchand, Roger, Gerald G. Mace, A. Gannet Hallar, Ian B. McCubbin, Sergey Y. Matrosov, and Matthew D. Shupe, 2013: Enhanced radar backscattering due to oriented ice particles at 95 GHz during StormVEx. *J. Atmos. Oceanic Technol*., **30**, 2336–2351.

Matrosov, S. Y., 2007: Modeling backscatter properties of snowfall at millimeter wavelengths. *J. Atmos. Sci*., **64**, 1727 – 1736.

Matrosov, S.Y., R.F. Reinking, R.A. Kropfli, B.E. Martner, and B.W. Bartram, 2001: On the use of radar depolarization ratios for estimating shapes of ice hydrometeors in winter clouds. J. *Appl. Meteor*., **40**, 479-490.

Matrosov, S.Y., A.J. Heymsfield, and Z. Wang, 2005a: Dual-frequency radar ratio of nonspherical atmospheric hydrometeors. *Geophys. Res. Lett*., **32**, L13816, doi:10.1029/2005GL023210.

Matrosov, S.Y., R.F. Reinking, and I.V. Djalalova, 2005b: Inferring fall attitudes of pristine dendritic crystals from polarimetric radar data. *J. Atmos. Sci*., **62**, 241-250.

Matrosov, Sergey Y., Gerald G. Mace, Roger Marchand, Matthew D. Shupe, Anna G. Hallar, Ian B. McCubbin, 2012: Observations of Ice Crystal Habits with a Scanning Polarimetric W-Band Radar at Slant Linear Depolarization Ratio Mode. *J. Atmos. Oceanic Technol*., **29**, 989–1008. doi:10.1175/JTECH-D-11-00131.175/JAS3904.1

Melnikov, V. and J.M. Straka, 2013: Axis ratios and flutter angles of cloud ice particles: Retrievals from radar data. *J. Atmos. Oceanic Technol*., **30**, 1691–1703.

Petty, G. W., and W. Huang, 2010: Microwave backscatter and extinction by soft ice spheres and complex snow aggregates. *J. Atmos. Sci*., **67**, 769–787.

Tyynela, J., J. Leinonen, D. Moisseev, and T. Nouslainen, 2011: Radar backscattering from snowflakes: Comparisons of fractal, aggregate and soft spheroid models. *J. Atmos. Oceanic Technol*., **28**, 1365-1372.

Zrnic., D., R. Doviak, G. Zhang, and A. Ryzhkov, 2010: Bias in differential reflectivity due to cross coupling through the radiation patterns of polarimetric weather radars. *J. Atmos. Oceanic Technol*., **27**, 1624-1637.